JAERI-M
6331

EXPERIMENTAL APPARATUS TO INVESTIGATE INTERACTIONS OF LOW ENERGY IONS WITH SOLID SURFACES

1. SUMMARY OF THE DESIGNS

December 1975

O. TSUKAKOSHI*, T. NARUSAWA*, M. MIZUNO*,
K. SONE, H. OHTSUKA, S. KOMIYA*

日本原子力研究所
Japan Atomic Energy Research Institute

JAERI-M 6331

Experimental Apparatus to Investigate Interactions of Low Energy Ions with Solid Surfaces

1. Summary of the Designs

Osamu TSUKAKOSHI*, Tadashi NARUSAWA*, Masayasu MIZUNO*,
Kazuho SONE, Hidewo OHTSUKA, Souji KOMIYA*

Division of Thermonuclear Fusion Research, Tokai, JAERI

(Received November 18, 1975)

Experimental apparatus to study the surface phenomena has been designed, which is intended to solve the vacuum wall problems in future thermonuclear fusion reactors and large experimental tokamak devices. An ion source and the beam transport optics are provided for bombarding solid target surface with an ion beam of energy from 0.1 to 6 keV. Measuring instruments include an ion energy analyser, a quadrupole mass spectrometer, an Auger electron spectrometer, an electro-micro-balance, a neutral particle energy spectrometer and its calibration system. Pumping system consists of oil-free ultrahigh vacuum pumps.

Various kinds of experiments will be carried out by using the apparatus: 1) sputtering by low energy ion bombardment, 2) re-emission of the incident particles during and after ion bombardment, 3) release of adsorbed and occluded gases in the solids by ion bombardment, and 4) backscattering of fast ions.

The combinations of measuring instruments for each experiment and their relative positions in the vacuum chamber are described through detailed drawings. The fundamental aspect in design of the ion beam transport optics for a low energy ion beam which can no longer neglect the space charge effect is also discussed.

---

* ULVAC Corporation, Hagisono 2500, Chigasaki-shi, Kanagawa-ken.

低エネルギースパッタリング実験装置

1. 設計の概要

日本原子力研究所東海研究所核融合研究部

塚越　修*，成沢　忠*，水野正保*，曽根和穂，大塚英男，
小宮宗治*

（1975年11月 18 日受理）

将来の核融合炉やそれを目標とした大型トカマクなどで予想され，または現実に解明しなければならない真空壁の表面現象の研究のための実験装置の設計を行った。本装置のイオン源およびビーム輸送系は，0.1～6 keV のエネルギー範囲のイオンビームで固体ターゲット表面を衝撃できるように設計されている。測定系を構成する主なものは，イオンエネルギー分析器，四重極質量分析計，電気微量天秤，中性粒子エネルギー分析器およびその較正系などである。また排気系はすべてオイルフリーの超高真空ポンプから構成されている。

本装置を用いることによって次のような多様な実験が可能となる。すなわち，固体ターゲットにおける 1)イオン衝撃によるスパッタリングの実験，2)イオン衝撃中の入射粒子再放出の実験，3）イオン衝撃による吸着・吸蔵ガス放出の実験，4)イオンの後方散乱の実験。

本報告では，これらの実験の測定系として使われる測定器の組み合わせおよび真空チェンバー内でのこれらの相互の位置関係について，詳細な図面を示しながら説明を加える。またイオン自身の空間電荷効果が無視できなくなる低エネルギー領域でのイオンビームの輸送系の設計に関する基本的な考え方を説明する。

＊　日本真空技術㈱ 技術開発部

目　次　な　し

1. Introduction

Impurity atoms in a plasma increase radiation losses, which result in breaking the energy balance and fading out the hope to establish thermonuclear fusion reactors. Recently, with improvement in characteristics of plasma confinement and with attainment of higher plasma temperature, the problems of plasma contamination by the influx of impurity atoms have been greatly closed up. Impurity atoms come mainly from the vacuum wall which is bombarded by the plasma, i.e. the wall is bombarded by energetic ions, neutral particles, fast neutrons, electrons and photons. Impurities are released from the wall by complicated processes including sputtering, blistering, local evaporation and desorption of adsorbed and occluded gases. Furthermore, for the particle balance of the plasma, surface phenomena such as backscattering of particles from the wall, trapping in the wall, re-emission and desorption of trapped gases play an important role.

The present experimental apparatus is designed in order to clarify experimentally these surface phenomena, and to measure the re-emission rate of impurities, the recycling rate of fuel ions and energy spectra of these particles. In this report, the authors describe detailed design of the devices and point out several new instruments adopted in the present experimental apparatus.

2. Main Parts of the Apparatus

A vacuum chamber (shown in Fig.1) has several ports which are usable to equip following devices:

1) Light gas ion gun and ion optics to produce H^+, D^+, He^+ and Ne^+ ion beams.

2) Metal ion gun and ion optics to produce metal ion beams; Mo^+, Nb^+, V^+, Fe^+, Ni^+ etc.

3) Ion energy analyser (IEA) and quadrupole mass spectrometer (QMS).

4) Cylindrical mirror Auger electron analyser (CMA).

5) Recording electro-micro-balance.

6) Neutral particle energy spectrometer (NPES) for backscattered neutrals and its calibration system.

7) Manipulators (2 sets) equipped with vacuum locks.

8) UHV pumps.

Devices 1) to 7) are located and adjusted as each axis intersects at the target within 1 mm diam. Devices 3) and 4) can be drawn 50 mm back from measuring positions to waiting ones without breaking vacuum. Devices 5) or 6) are alternatively mounted at the top port. Fig.2 shows an experimental arrangement in which devices 1), 3) and 7) are mounted on the vacuum chamber for gas release rate measurement during ion (H^+, D^+ or He^+) bombardment.

3. Details of the Combinations of Measuring Instruments

3.1. Sputtering Yield Measurements for Solid Targets by Low Energy Ions

Measurements are done by two methods; 1) absolute yield measurement by the recording electro-micro-balance, and 2) sensitive detection of sputtered atom coverage by Auger electron spectroscopy,

as shown in Figs.3 and 4, respectively.

3.1.1. Absolute Yield Measurement by the Recording Electro-micro-balance

A target of 30 mm diam. is bombarded by a low energy ion beam as shown in Fig.3. Sputtered atoms are deposited inside of a bell-shaped collector of 35 mm diam. and weighed by the recording electro-micro-balance*. The angle of incidence for the primary ion beam to the normal of the target surface is variable in the range of 0° to 75°. The collector is made of thin glass of 0.1 mm thick and its inner surface is coated with a gold film. The collector has an aperture of 9 mm diam. to pass the primary ion beam. The adjustment of the aperture to the primary ion beam axis is carried out by putting the bell-shaped collector on an annular disk and rotating it by the vertically mounted manipulator as shown in Fig.3.

When the primary ion beam current is assumed to be 60 μA for H^+ and the target molybdenum, the minimum detectable sputtering yield for this method is as follows.

The minimum detectable weight change of the electro-micro-balance is 5×10^{-7}g. Assuming a collection duration of 1 hr and a collection efficiency of 90% in total sputtered Mo atoms, the sputtering yield S_1 to reach the minimum detectable weight change of 5×10^{-7}g is given by

$$S_1 \times \frac{6 \times 10^{-5}\ [A]}{1.6 \times 10^{-19}\ [\text{Coulomb}]} \times 3.6 \times 10^{3}\ [\text{sec}] \times 0.9 = \frac{5 \times 10^{-7}\ (g) \times 6 \times 10^{23}}{95.95\ [g]},$$

$$\text{or } S_1 = 2.6 \times 10^{-3} \text{ atoms/ion.}$$

*Cahn electro-micro-balance, type RG-UHV

3.1.2. Relative Yield Measurement by AES

Sputtered atoms are collected on a substrate which is located apart 20 mm from the target as shown in Fig.4 (a). Impurities on the target surface are detected with CMA* by rotating the target 120° from the bombarding position (Fig.4 (a)) to the measuring one as shown in Fig.4 (b).

This enables us to ensure cleanliness of the target surface before, during or after ion bombardment. The substrate is carried to CMA by rotating with the horizontally mounted manipulator when the measurement of Auger peaks of deposited layers on the substrate after a given time of sputtering is carried out as shown in Fig.4 (c). A target is cleaned by a repeated cycle of high-temperature annealing up to 1700°K and Ne^+ ion bombardment with the ion energy of 2 keV. The Ne^+ ion beam is produced by alternative use of the light gas ion gun and its ion optics.

When the target is molybdenum a tungsten substrate is adopted as this combination is well analysed by Tarng and Wehner.[1] The minimum detectable surface coverage of Mo by CMA is 1.4×10^{-3} monolayers. When the primary ion beam current and the target are assumed to be the same as in the previous method described in 3.1.1 , the sputtering yield S_2 to reach the minimum detectable coverage within 1 hr is given by

$$S_2 \times \frac{6 \times 10^{-5}\ [A]}{1.6\times10^{-19}[\text{Coulomb}]} \times 3.6\times10^{3}[\text{sec}] \times \frac{1}{2\pi 2^2[\text{cm}^2]}$$

$$= 1.4\times10^{-3} \times 1.11 \times 10^{15}[\text{atoms/cm}^2], \text{ or } S_2 = 2.9\times10^{-5} \text{ atoms/ion.}$$

---

* Physical Electronics Ind. Model 10-155

Absolute measurements of the sputtering yield versus ion energy are available in the range of relatively high region of the yield ($\gtrsim 10^{-2}$ atoms/ion) by the electro-micro-balance and the yield near the threshold is measured by CMA. The criterion and the expected results are shown in Fig.5.

3.2. Re-emission, Backscattering and Occluded Gas Release during Light Ion Bombardment

3.2.1. IEA and QMS: Measurement of Ion Energy Distributions

Energy distributions of sputtered ions and released gas ions are measured by a combination of the ion energy analyser (IEA) and the quadrupole mass spectrometer (QMS) as shown in Fig.6.

Distance from the target to the inlet of IEA: 30 mm.
Energy resolution of IEA: $\Delta E/E=10\%$(at E=50 eV).
Mass resolution of QMS: $M/\Delta M=500$(10% valley definition).

IEA and QMS are isolated electrically from the target and the vacuum chamber, and they are operated at 0 to 500 V with respect to the ground potential while the energy resolution is kept constant to be a few volts. Therefore, the ion energy distributions can be measured between 0 to 500 eV for each m/e.

3.2.2. NPES: Measurement of Energetic Neutrals and Ions

Backscattered ions and neutrals which have the energy higher than 200 eV are measured by a neutral particle energy spectrometer (NPES). NPES consists of a stripping cell which is filled with nitrogen gas of approximately 2×10^{-3} Torr, a deflector and an

electrostatic energy analyser. In the measuring position, NPES is alternatively mounted at the top port which is used for the electro-micro-balance. In the calibration of neutral to ion conversion efficiency versus neutral particle energy, NPES will be located at the uniaxial direction with the axis of the light ion beam optics as roughly shown in Fig.1 (b). For the calibration, the primary ion beam is neutralized by another charge transfer cell which is filled with oxygen gas of approximately 2×10^{-3} Torr. Counting rate of approximately 10^4 cps for neutral hydrogen atoms which have the kinetic energy of 200 eV will be possibly expected by proton beam of 60 μA. The criterion and expected results are shown in Fig.7.

3.2.3. Measurement of Released Gases

Fig.8 shows the experimental set-up for the measurement of released gases during ion bombardment and thermal desorption spectra of trapped species. A combination of an enclosed ionization chamber and QMS is adopted to detect gas evolution rate. Gas molecules released from the target are accumulated in a hemi-spherical volume of 30 mm diam. and analysed. The target can be annealed up to 1700°K which is sufficient to erase the memory of the previous ion bombardment. A temperature range of thermal desorption will be set from room temperature to 800°K. Energetic particle impacts cause gas release, trapping and build-up of the temperature at the inner wall of the closed volume, which may introduce experimental errors. In order to minimize these errors, the inner wall is occasionally covered with a clean gold film. An evaporation source is mounted on the

horizontal manipulator and moved to be located at the position to evaporate gold on the surface of the inner wall. Pumping of the closed chamber is carried out through the aperture of 9 mm dia. through which the primary beam passes. The effective conductance of this aperture for nitrogen is 9.53 ℓ/sec. A gas evolution rate Q_o [Torr·ℓ/sec] at t_o[sec] after start of the ion bombardment is expressed as

$$Q_o = p_o S/[1 - \exp(-\frac{S}{V} t_o)],$$

where S is the effective pumping speed. If V is assumed to be 0.5ℓ which includes the volume of the closed chamber, the ionization chamber and QMS, and if the minimum detectable partial pressure level p_o and build-up time t_o is assumed to be 5×10^{-10} Torr and 0.1 sec, respectively, Q_o is given by

$$Q_o = 5.6 \times 10^{-9} \text{ Torr·ℓ/sec.}$$

This value of Q_o corresponds to 1.9×10^{11} molecules/sec. The minimum detectable gas release rate by this method is

$$\eta_{N_2} = 4.9 \times 10^{-4} \text{molecules/ion.}$$

3.3. Pumping System

The pumping system consists of two sputter ion pumps, two cryo-pumps, a turbo molecular pump, a roots pump, a rotary pump and tubings as shown in Fig.9. The ion source and the beam transport system are pumped differentially through three orifices. The main chamber is evacuated by a combination of a cryo-pump and a sputter ion pump. In order to increase the pumping speed of

the cryo-pump for hydrogen gas, the temperature of the cryo-surface must be below 2.4°K, reaching the saturated hydrogen vapor pressure which is negligible even in UHV. To obtain 2.4°K the pressure in the liquid helium vessel is reduced by a mechanical pump. The working pressure in the main chamber is expected to be lower than 1×10^{-9} Torr.

4. Design of Ion Beams

4.1. Requirements for the Design of Ion Beams

The design of ion beams was carried out under the following considerations.

1) Two stages of differential pumping are indispensable for the present arrangement to carry out experiments.

2) When a proton beam is used as the primary ion beam, the ion energy of 100 eV to 6 keV and the ion current of 50 to 100 μA are required at the target. The spread of ion beams caused by the space charge effect of ions in a field free space is serious in lower ion energy regions, for instance, for the proton beam with energy of 100 eV and ion current of 60 μA. In order to avoid the ion beam spread by the space charge effect, it is necessary to transport the beam with energy of 500 eV to 3 keV from the ion source to the electrode in front of the target.

3) Mass separation is indispensable for the arrangement to measure the sputtering yield by proton bombardment, as the sputtering yields for H^+ and H_2^+ differ approximately by a factor of 2, and furthermore, heavy impurity ions would cause serious errors. Therefore, it is decided to insert a magnetic

sector type mass analyser and to design the mass analyser capable of stigmatic focusing of the ion beam (which is discussed in 4.2.2).

4.2. Detailed Design of Ion Beams

We explain briefly for the case of the proton beam with energy of 100 eV. The notation of electrodes and applied voltages are shown in Fig.10.

1) A proton beam is extracted by the electrode EL1 from the expansion cup of the duoplasmatron (which is held at a potential of 100 V from the earth) and focused to the slit EL4 by the cylindrical lens EL2 and EL3. A computer estimation of the contour of the proton beam in this cylindrical lens is shown in Fig.11. In this case, potentials of the ion source EL0, EL1, EL2, EL3 are equal to 100 V, -2.9 kV, -5.9 kV and -400 V, respectively.

2) The design of magnetic sector type mass analyser is as follows.

i) Deflection angle of the analyser: 90°.

ii) Orbital radius in the magnetic field: 12 cm.

iii) Both α-and ω-focusing are possible. The α-focusing is attained by focusing properties of the sector magnet, and the ω-focusing is by the two-dimensional lenses (EL5, EL6 and EL7) and (EL7, EL8 and EL9) shown in Fig.10. The stigmatic focusing will be expected by this arrangement.

iv) A part of the two-dimensional lens EL7 is thrusted into the sector section envelope and the potential VL7 of -1600 V is given to it. The proton beam passes through the mass analyser with the kinetic energy as large as 1700 eV. A computer

simulation of the contour of the proton beam in the two-dimensional lens is shown in Fig.12. In this case the voltages VL6 = -400 V and VL7 = -1600 V are applied to a pair of electrodes of the two-dimensional lens, respectively.

3) To electrodes EL10, EL11 and EL12 of the second cylindrical lens, the voltages are applied as follows:
VL10 = -400 V, VL11 = -2400 V, VL12 = -400 V, so that the proton beam is focused at the slit EL13. A contour of the proton beam in the cylindrical lens is shown in Fig.13.

4) The third cylindrical lens consists of the electrodes EL14, EL15 and EL16. Those are similar to the description in the previous paragraph. An end cap EL17 is held at the earth potential. The proton beam is sent into field free region through EL17 to the target. The end cap EL17, together with EL16, composes a diaphragm lens and shows a focusing property of the ion beam. A computer simulation based on the data obtained by an electrolytic tank experiment[2] is shown in Fig.14. Typical voltages applied to electrodes to obtain the proton beams of 100 eV and 6 keV are shown in Fig.10. In the case of the 100 eV proton beam, the expansion cup EL0 and the final electrode EL16 are kept at 100 V and -400 V, respectively, while the end cap EL17 is at earth potential.

The apparatus is now being fabricated at ULVAC Corporation, and the experiments for low energy proton and deuteron beams incident onto Mo targets will be begun April 1976.

Acknowledgements

The authors are much indebted to Dr. S.Mori, Director of Division of Thermonuclear Fusion Research, JAERI and Dr. C.Hayashi, President of ULVAC Corporation for their initial theme setting and permission to publish the present paper. The authors would like to thank Drs. M.Yoshikawa, K.Shiraishi, H.Shirakata, T.Tazima, Division of Thermonuclear Fusion Research, JAERI and Y.Gomay, guest scientist from Toshiba Central Lab. for their early stage guidance and continuous encouragements. The authors are also much indebted to Prof. G.K.Wehner (Minnesota Univ.), Dr. R.Behrisch (Max-Planck Institute, Garching) and Dr. P.W.Palmberg (Physical Electronics Industries) for their valuable discussions.

APPENDIX

Calculations on Contours of Ion Beams

A computer-aided design of ion beams in a cylindrical lens, in a two-dimensional lens and through decelerating or accelerating lenses are carried out by taking into account the space charge effect.

1. Contour of Ion Beam in a Cylindrical Lens

1.1. Paraxial Ray Equation in Axially Symmetric Field by Taking into Account the Space Charge Effect

We describe the motion of an ion in the beam by cylindrical polar co-ordinates by taking the symmetrical axis as z-axis. When we assume that the potential $\phi(r,z)$ can be expanded as polynomials of r,

$$\phi(r,z) = \sum_{n=0}^{\infty} a_n(z) r^n. \qquad (1.1)$$

From the condition of axial symmetry,

$$a_{2n+1}(z) = 0 \qquad (n=0,1,2, \ldots\ldots\ldots). \qquad (1.2)$$

By putting eqs. (1.1) and (1.2) into Poisson's equation given by

$$\frac{\partial^2\phi}{\partial z^2} + \frac{\partial^2\phi}{\partial r^2} + \frac{1}{r} \cdot \frac{\partial\phi}{\partial r} + \frac{\rho}{\varepsilon_0} = 0,$$

and by neglecting higher order terms of r,

$$\phi(r,z) = V(z) - \frac{1}{4}(V''(z) + \rho/\varepsilon_0)r^2 \qquad (1.3)$$

where ρ is the density of space charge caused by ions, ε_0 is the permittivity of vacuum, V(z) is the electrostatic potential on z-axis, and '' means differenciating twice with z. Thus we obtain the equation of motion of an ion in the beam as follows:

$$\ddot{r} = -\frac{e}{m}\frac{\partial\phi}{\partial r} = \frac{\eta}{2}(V''(z) + \rho/\varepsilon_0)r,$$

where η is equal to charge to mass ratio e/m of the ion in question. On the other hand, r can be rewritten as follows:

$$\dot{r} = \frac{dr}{dz}\cdot\frac{dz}{dt} = r'\dot{z}, \quad \ddot{r} = r''\dot{z}^2 + r'\ddot{z},$$

where ' means differentiation with z. From the paraxial condition, as $|\dot{r}| \ll |\dot{z}|$, $\dot{z}$ can be written by

$$\dot{z}^2 = \dot{r}^2 + \dot{z}^2 = \frac{2e}{m}[V_0 + \phi_{init} - \phi(r,z)],$$

where ϕ_{init} is the electrostatic potential at the starting point of the ion, and eV_0 is the kinetic energy at the same point. From the equation of motion given by

$$\ddot{z} = -\frac{e}{m}\cdot\frac{\partial\phi}{\partial z} = -\eta V'(z),$$

$\ddot{r}$ can be rewritten as follows:

$$\ddot{r} = r''2\eta(V_0 + \phi_{init} - V(z)) + r'(-\eta V'(z)). \qquad (1.5)$$

Assuming that the charge density is homogeneous to the direction of radius, and that r is the radius of the contour of the ion beam, we obtain

$$\rho = I/\pi r^2 \cdot \dot{z} = I/\sqrt{2}\pi\eta^{1/2}(V_o + \phi_{init} - V(z))^{1/2} r^2. \qquad (1.6)$$

From eqs. (1.4), (1.5) and (1.6) we obtain

$$r'' + \frac{V'r'}{2(V-V_o-\phi_{init})} + \frac{V''r}{4(V-V_o-\phi_{init})} - \frac{I \cdot \frac{1}{r}}{4\sqrt{2}\pi\varepsilon_o\eta^{1/2}(V_o+\phi_{init}-V)^{3/2}} = 0. \qquad (1.7)$$

Putting recommended consistent values of the fundamental constants described in CODATA Bulletin[3] into eq. (1.7), we obtain

$$\frac{d^2r}{dz^2} + \frac{dV/dz \cdot dr/dz}{2(V-V_o-\phi_{init})} + \frac{d^2V/dz^2 \cdot r}{4(V-V_o-\phi_{init})}$$

$$- 0.64699 \times 10^6\sqrt{M_u}\,\frac{I \cdot \frac{1}{r}}{(V_o+\phi_{init}-V)^{3/2}} = 0, \qquad (1.8)$$

(M_u: mass number; V_o, V, ϕ_{init} in volt; I in ampere).

1.2. Paraxial Ray Equation in a Cylindrical Lens Composed of Two Cylindrical Electrodes with Equal Diameter by Taking into Account the Space Charge Effect

We take the middle point on the axis between two cylindrical electrodes as the origin of cylindrical co-ordinate, and introduce the following normalized co-ordinates by

$$R = r/r_o, \quad Z = z/r_o,$$

where r_o is the radius of cylindrical electrode. The potential on the axis is given by the following formula:[4,5]

$$V(Z) = \frac{1}{2}(V_1 + V_2) + \frac{1}{2}(V_1 - V_2)\tanh wZ, \qquad (1.9)$$

$$w = 1.318,$$

where V_1 and V_2 are the potentials applied to the electrodes of the cylindrical lens as shown in Fig.15. From eqs. (1.8) and (1.9) the following differential equation can be obtained for the case when $V_o + \phi_{init}$ vanishes:

$$\frac{d^2R}{dZ^2} + 0.659 \cdot F \cdot \frac{dR}{dZ} - 0.868562 \cdot R \cdot F \cdot \tanh wZ$$

$$- 0.64699 \times 10^6 \sqrt{M_u} \cdot I \cdot \frac{1}{R} / (-V)^{3/2} = 0, \qquad (1.10)$$

and

$$F = \frac{1 - V_1/V_2}{\cosh^2(wZ)\ (1 + V_1/V_2 + (1 - V_1/V_2)\tanh wZ)}. \qquad (1.11)$$

When $V_o + \phi_{init}$ does not vanish, we substitute $V_1 - V_o - \phi_{init}$ and $V_2 - V_o - \phi_{init}$ for V_1 and V_2, respectively in eq. (1.11), and calculate the contour of the beam from eq. (1.10).

1.3. Focusing Properties of the Cylindrical Lens When the Space Charge Effect Can be Neglected

The successive integrations of the differential equation (1.10) are carried out numerically by employing a computer as follows:

$$DR(1) = \left(\frac{dR}{dZ}\right)_{Z=Z_1} = \left(\frac{dR}{dZ}\right)_{Z=Z_0} + \left(\frac{d^2R}{dZ^2}\right)_{Z=Z_0} (Z_1 - Z_0),$$

and

$$R(1) = R(Z=Z_1) = R(Z=Z_0) + DR(1)\ (Z_1 - Z_0).$$

To check the validity of the method, the focusing properties of the cylindrical lens are calculated when the space charge effect can be neglected by assuming that the last term in eq.(1.10) vanishes. The results are compared with the data reported by Nattali, Kuyatt et al.[6] which have been known to be accurate within the error less than 10^{-4}. Four kinds of focal lengths are calculated for cylindrical lenses as shown in Fig.16. The result is shown in Table 1.

The contour of the ion beam in field free region are also calculated by assuming that V_1 is equal to V_2 and consequently F is null in eq. (1.10). The present result agrees well with the result calculated manually by the method described by Pierce.[7]

1.4. Contour of Ion Beam in a Cylindrical Lens by Taking into Account the Space Charge Effect

The procedure described in 1.2 and 1.3 is sufficiently accurate to carry out the design of ion beam with the parameters adequate for practical design. Several results are shown in Fig.17 and Fig.18. The reversibility of the ion beam in cylindrical lens is still conserved even under the influence of the space charge.

2. Contour of Ion Beam in a Two-dimensional Lens

It is possible to obtain the paraxial ray equation in the electrostatic field with two-dimensional symmetry. When the

symmetrical axis is taken as z-axis, the following differential equations are obtained:

$$\frac{d^2y}{dz^2} + \frac{dV/dz \cdot dy/dz}{2(V - V_o - \phi_{init})} + \frac{d^2V/dz^2 \cdot y}{2(V - V_o - \phi_{init})}$$

$$- \frac{I}{w} \frac{1}{4\sqrt{2}\,\varepsilon_o \eta^{1/2} (V_o + \phi_{init} - V)^{3/2}} = 0 , \qquad (2\text{-}1)$$

or

$$\frac{d^2y}{dz^2} + \frac{dV/dz \;\; dy/dz}{2(V - V_o - \phi_{init})} + \frac{d^2V/dz^2 \cdot y}{2(V - V_o - \phi_{init})} - \frac{I}{w} \frac{0.2032579 \times 10^7 \sqrt{M_u}}{(V_o + \phi_{init} - V)^{3/2}} = 0, \qquad (2\text{-}2)$$

where w is the width of the beam in the direction of x, V, V_o, ϕ_{init} are the potentials in [V], I is the total current of the beam in [A] and M_u is the mass number.

The electrostatic potential composed of two pairs of semi-infinite planes (Fig.19) is given by[8)]

$$V = V_1 \left[\frac{V_2}{V_1} + \left(1 - \frac{V_2}{V_1}\right)\left(\frac{1}{\pi}\right)\left\{\tan^{-1} \frac{\cos \pi y/d}{\sinh \pi z/d} + \pi\right\}\right] , \text{ for } z \leq 0 \qquad (2.3)$$

$$V = V_1 \left[\frac{V_2}{V_1} + \left(1 - \frac{V_2}{V_1}\right)\left(\frac{1}{\pi}\right) \tan^{-1}\left(\frac{\cos \pi y/d}{\sinh \pi z/d}\right)\right] , \text{ for } z \geq 0 \qquad (2.4)$$

$-d/2 \leq y \leq d/2.$

These formulas satisfy both boundary conditions and Laplace's equation and thus the analytical solution of the given arrangement We normalize y, z and w by d and write as follows:

$$Y = y/d, \quad Z = z/d, \quad W_n = w/d \qquad (2.5)$$

We obtain the following differential equation for the contour of the paraxial beam in two-dimensional lens by taking into account the space charge effect when $V_o + \phi_{init}$ vanishes:

$$\frac{d^2Y}{dZ^2} - \frac{(1-\frac{V_2}{V_1})\frac{\cosh\pi Z}{1+\sinh^2\pi Z}\frac{dY}{dZ}}{2[\frac{V_2}{V_1}+(1-\frac{V_2}{V_1})(\frac{1}{\pi})\{\tan^{-1}(\frac{1}{\sinh\pi Z})_{+o}^{+\pi}\}]}$$

$$+\frac{(1-\frac{V_2}{V_1})\pi\sinh\pi Z\cosh^2\pi Z/(1+\sinh^2\pi Z)^2}{2[\frac{V_2}{V_1}+(1-\frac{V_2}{V_1})(\frac{1}{\pi})\{\tan^{-1}(\frac{1}{\sinh\pi Z})_{+o}^{+\pi}\}]}\,Y$$

$$-\frac{I}{W_n}\frac{0.2032579\times10^7\sqrt{M_u}}{[-\frac{V_2}{V_1}-(1-\frac{V_2}{V_1})(\frac{1}{\pi})\{\tan^{-1}(\frac{1}{\sinh\pi Z})_{+o}^{+\pi}\}]^{3/2}}=0\,. \qquad (2\text{-}6)$$

In the above equation we add $+\pi$ to $\tan^{-1}(\frac{1}{\sinh\pi Z})$ for $Z \leq 0$, and add nothing for $Z \geq 0$.

Focal lengths of a two dimensional lens are calculated when the space charge effect can be neglected by a procedure similar to that described in 1.3 and the present results agree well with the results obtained by Pierce.[9] The contour of the beam in the field free region is calculated by assuming that V_1 is equal to V_2, and it agrees well with the contour calculated manually by the procedure described by Pierce.[10] The contour is calculated under the condition that the beam width w increases linearly with z. Several examples are shown in Fig.20. The reversibility of the ion beam in a two-dimensional lens is still conserved even under the influence of space charge.

3. Contour of Ion Beam through an Electrostatic Lens Composed of Two Thin Annular Disks

Calculation of the contour of an ion beam in an axially symmetric electrostatic field obtained from the electrolytic tank experiment is carried out on the basis of the paraxial ray equation by taking into account the space charge effect.

The following procedure is adopted to calculate the contour of the ion beam through a practical lens. A semicircular arrangement analogous to the practical arrangement of electrodes is made, and the distribution of electrostatic potential on the axis of symmetry is measured by the electrolytic tank method.[2] The calculation of the contour of the ion beam is made by employing the following program of computer.

1) The contour of the ion beam is calculated by successive integration of eq. (1.8) by the method described in eq. (1.3), where V, dV/dz and d^2V/dz^2 are calculated from the data obtained by the electrolytic tank experiment by the following procedure as described in the following paragraph 2).

2) Corresponding to the point where successive integration is being carried on, we take nearest four data points:

(z_{i+1}, V_{i+1}), (z_{i+2}, V_{i+2}), (z_{i+3}, V_{i+3}) and (z_{1+4}, V_{i+4}),

and simulate the distribution of the electrostatic potential on the axis with a quadratic polynomial of z as follows:

$$V(z) = V_o + A(z-z_0)^2 + B(z-z_0) + C,$$

$$V_o = \frac{1}{4} \sum_{j=i+1}^{i+4} V_j ,$$

$$z_0 = \frac{1}{4} \sum_{j=i+1}^{i+4} z_j \ ,$$

where A, B and C are determined by the least square method.

From this quadratic formula, we calculated V, dV/dz and d^2V/dz^2.

Several examples obtained by this procedure are shown in Fig.21.

References

1) M.L.Tarng and G.K.Wehner, J. Appl. Phys., 44 (1973) 1534.

2) P.Grivet, "Electron Optics" (Pergamon Press, New York, 1965) p.21.

3) CODATA Bulletin, No.11 (1973).

4) S.Bertram, Proc. Inst. Radio Engineering, 28 (1940) 418.

5) T.Mulvey and M.J.Wallington, Rep. Prog. Phys., 36 (1973) 359.

6) S.Nattali, D.DiChio, E.Uva and C.E.Kuyatt, Rev. Sci. Instrum., 43 (1972) 80.

7) J.R.Pierce, "Theory and Design of Electron Beams" (D. Van Nostrand Company, New York, 1954) p.147.

8) J.R.Pierce, ibid., p.107.

9) J.R.Pierce, ibid., p.112.

10) J.R.Pierce, ibid., p.151.

Table 1. Comparison of calculated focal lengths of a cylindrical lens.

V_2/V_1	F_1/r_o		FF_1/r_o		F_2/r_o		FF_2/r_o	
	Present study	N-K	Present study	N-K	Present study	N-K	Present study	N-K
2	25.9007	26.2654	21.6833	21.983	25.65115	25.8112	30.5698	30.888
2.5	——	15.3312	——	12.0626	——	14.988	——	19.0692
3	——	10.8962	——	8.131	——	10.6864	——	14.0832
4	7.02491	——	4.79611	——	6.49446	——	9.56553	——
5	5.43241	5.5366	3.44668	3.5148	4.81968	4.9318	7.68658	7.8592
6	4.55883	——	2.71651	——	3.87819	——	6.63678	——

N-K: Results obtained by Nattali, Kuyatt et al.

JAERI-M 6331

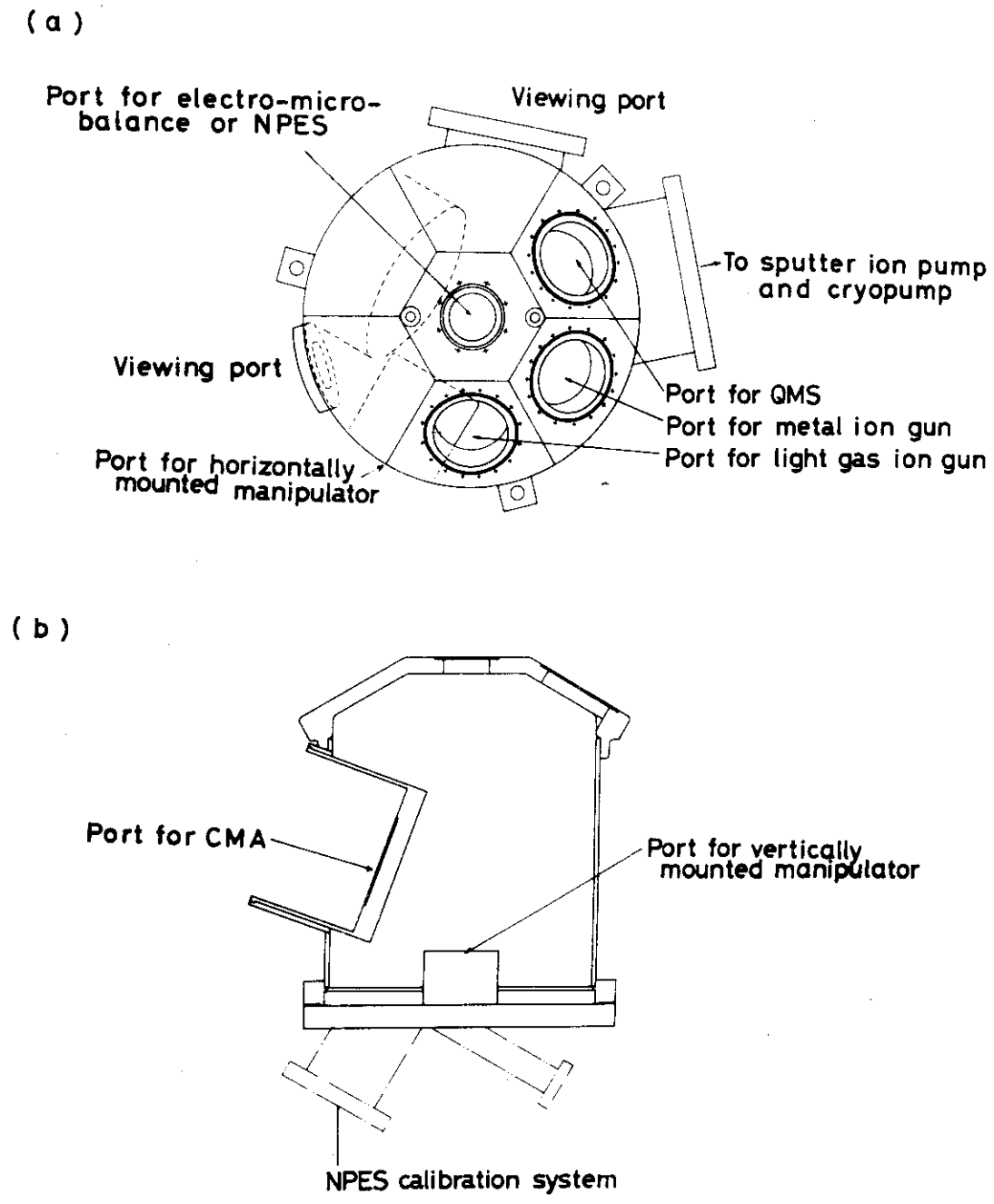

Fig.1 Vacuum chamber.

a) top view,
b) side view.

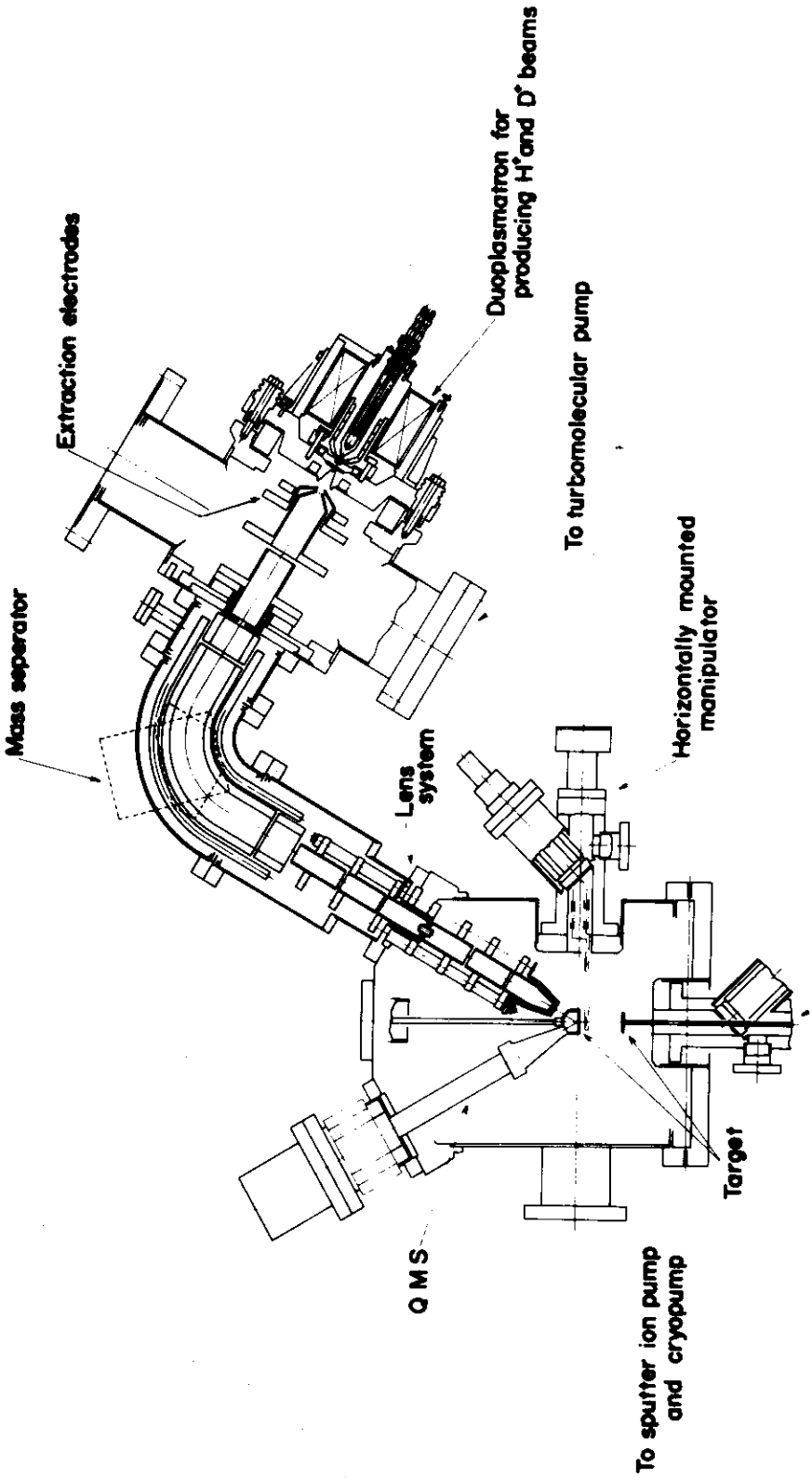

Fig.2 Experimental arrangement for gas release rate measurement.

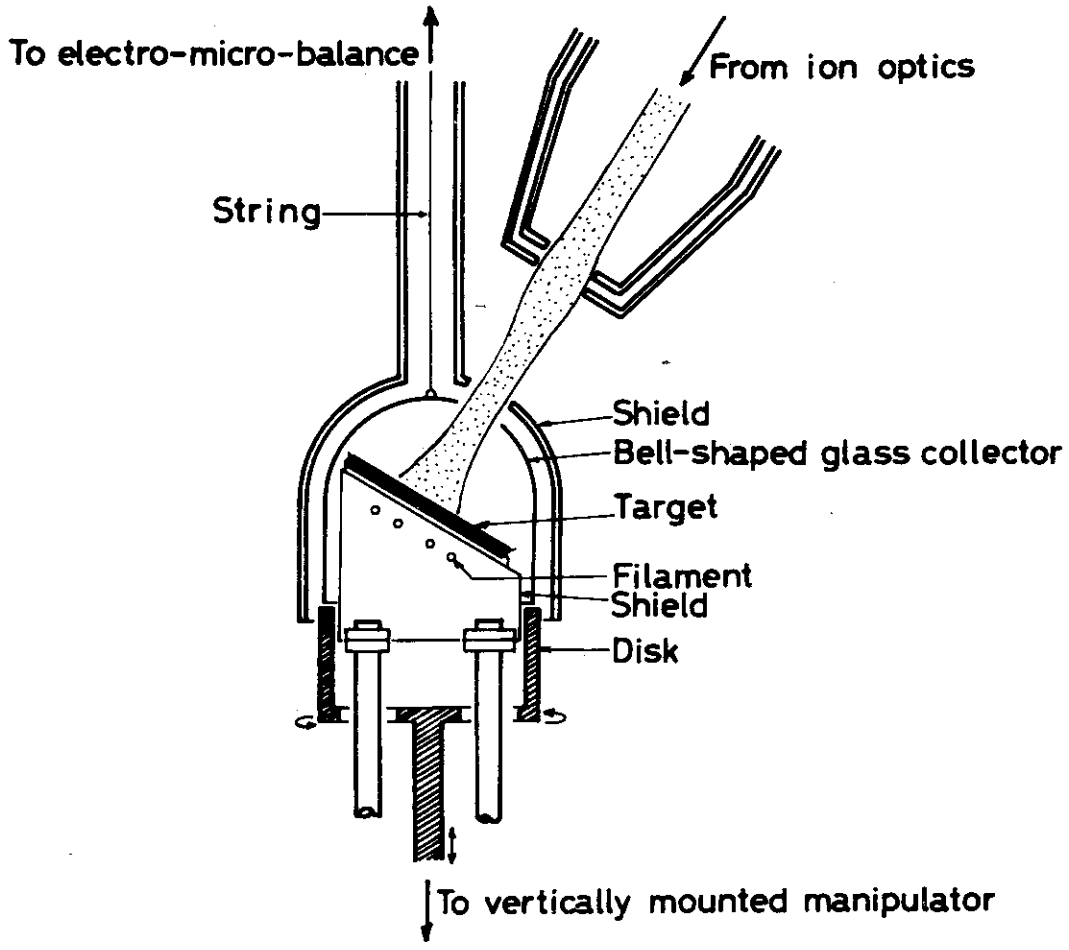

Fig.3 Set-up for absolute sputtering yield measurement by recording electro-micro-balance.

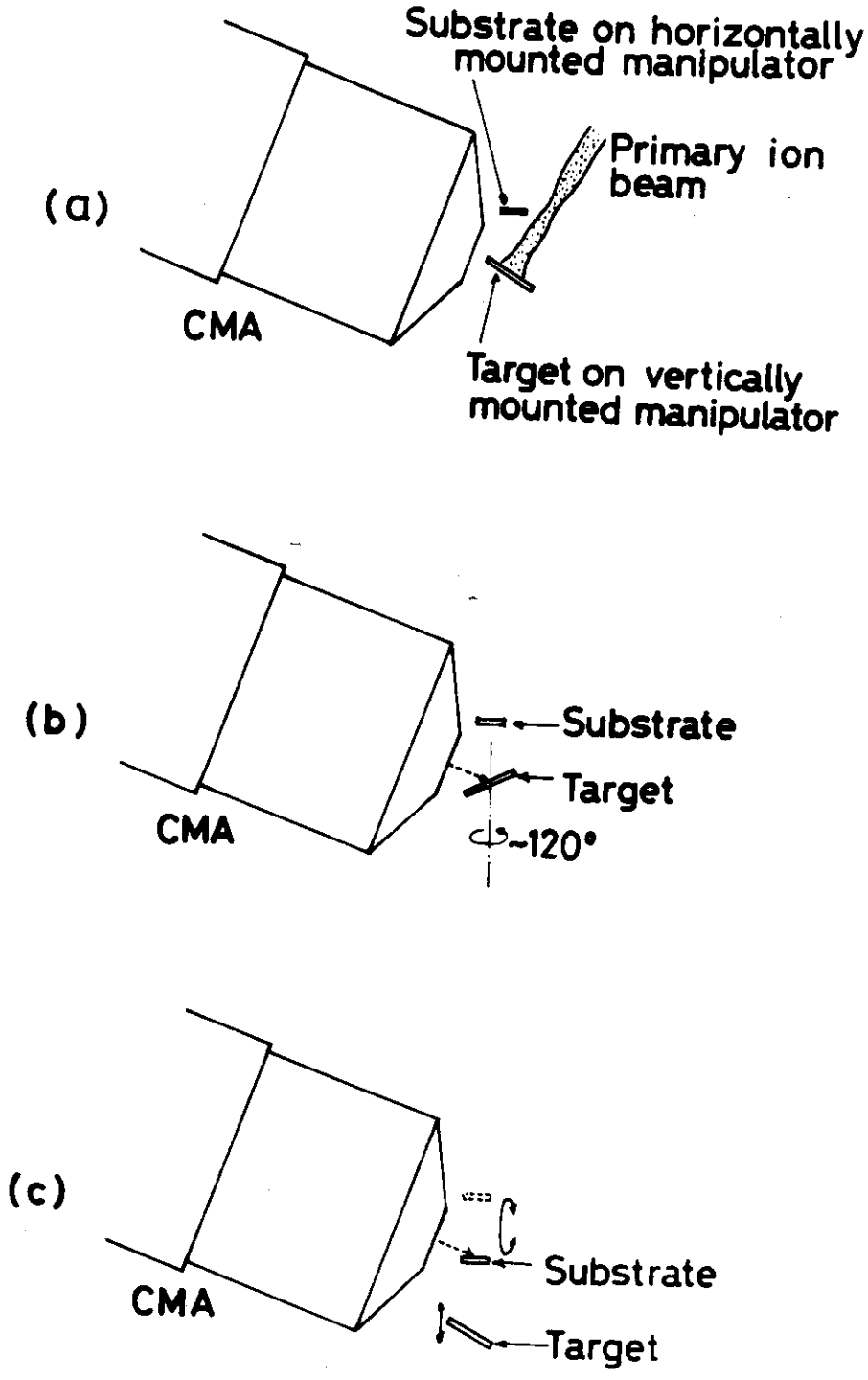

Fig.4 Set-up for relative sputtering yield measurement by AES.

a) depositing position,
b) detecting position for impurity on target surface,
c) measuring position.

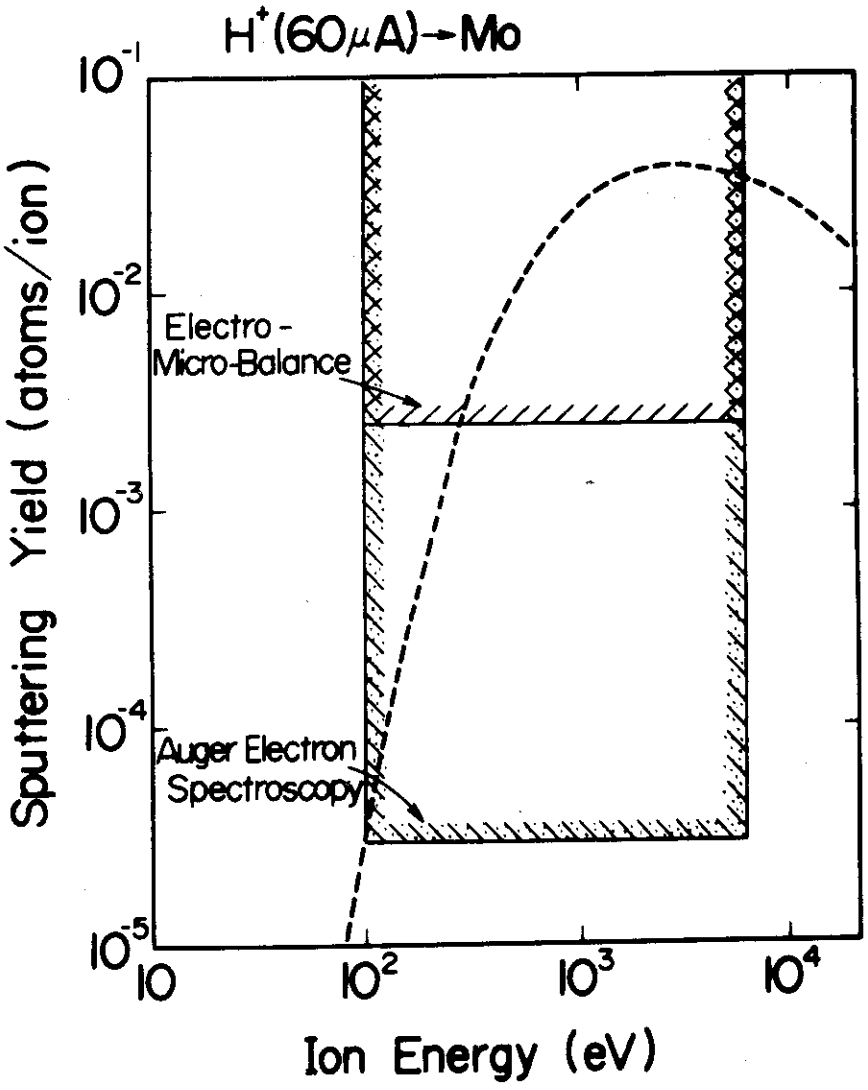

Fig.5 Measurable criterion and expected sputtering yield for H^+ incident on molybdenum target.

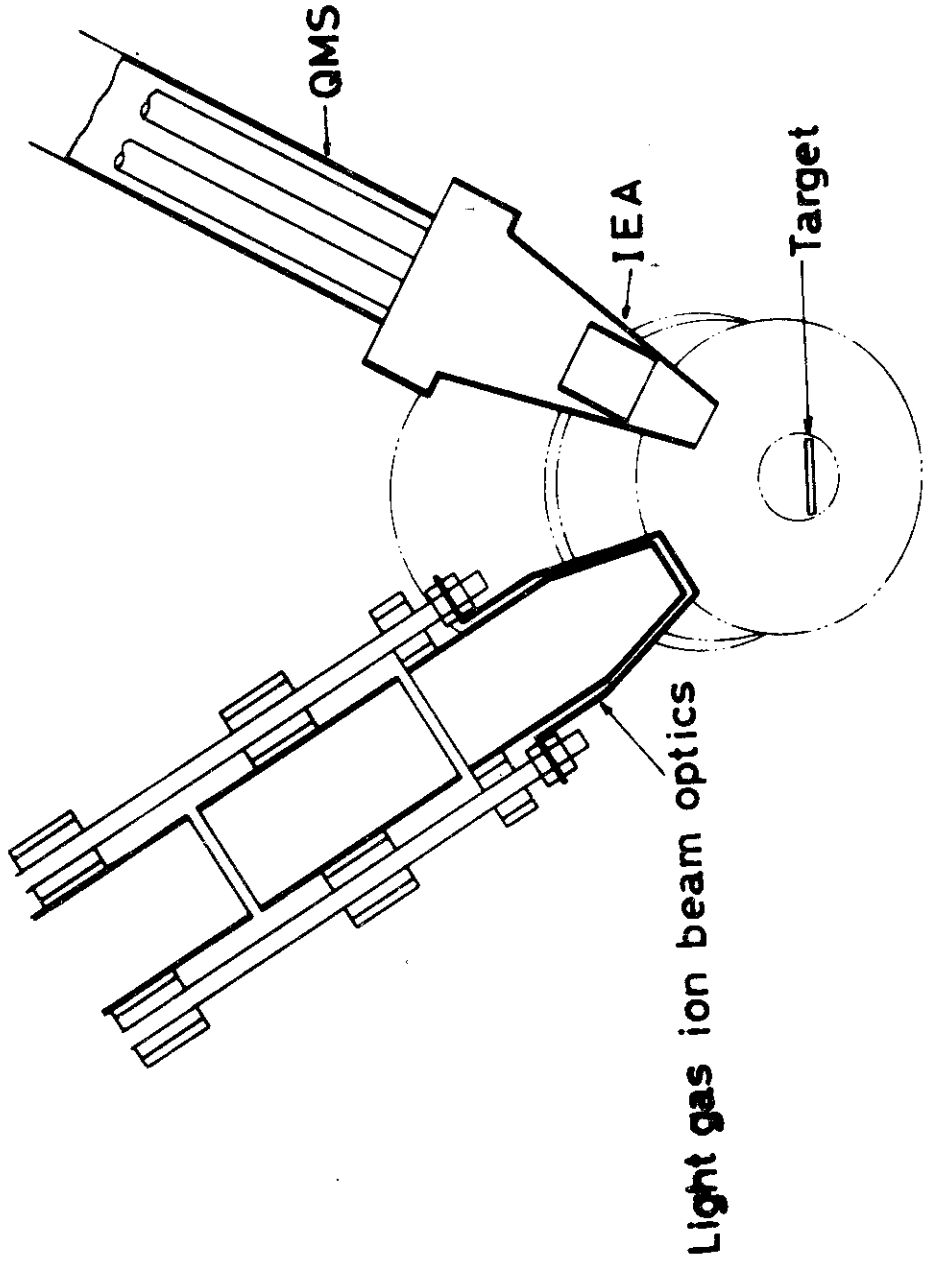

Fig.6 Set-up for measurement of sputtered metal ions and released gas ions by SIMS.

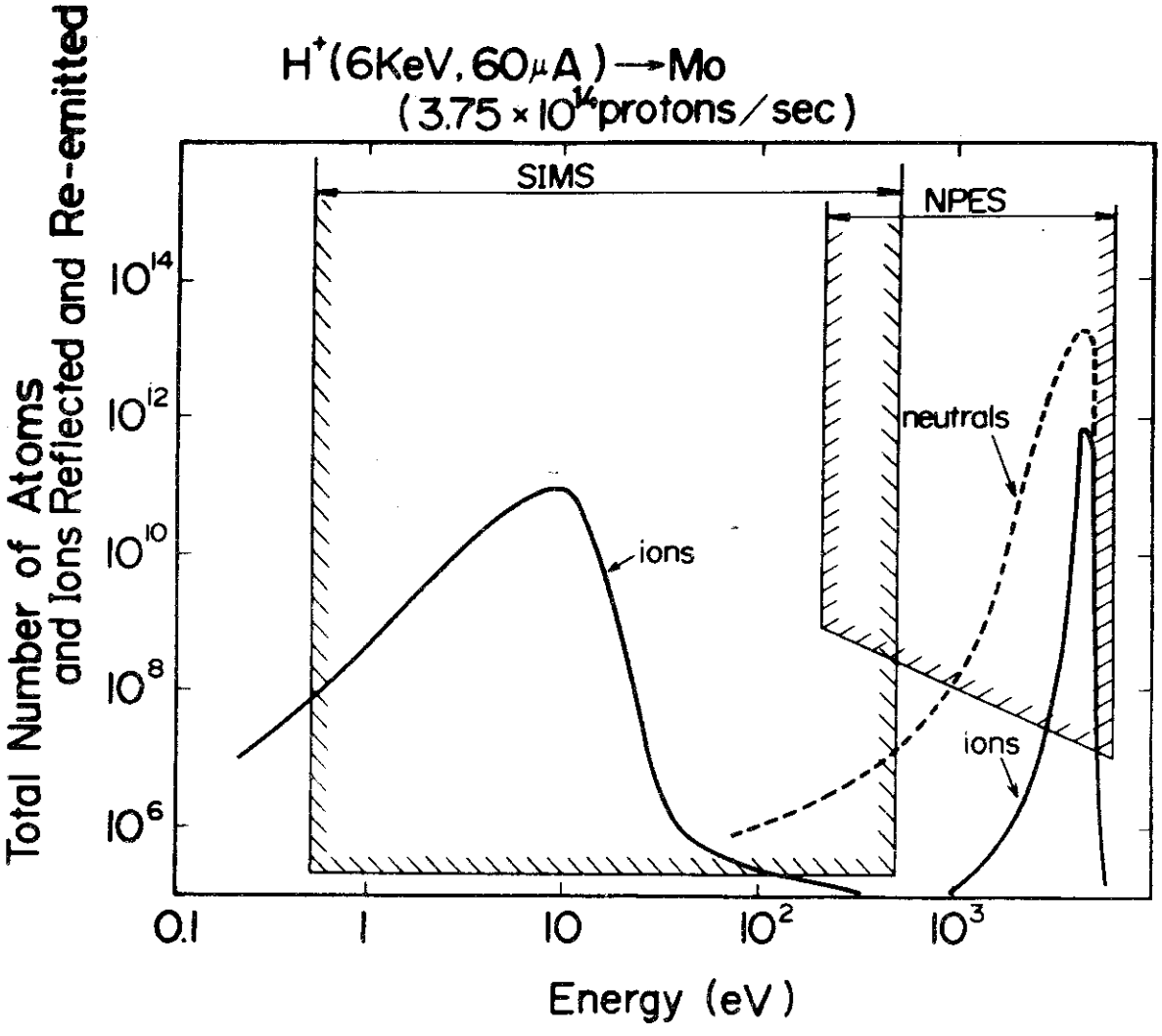

Fig.7 Measurable criterion and expected ion energy spectra for H^+ incident on molybdenum target.

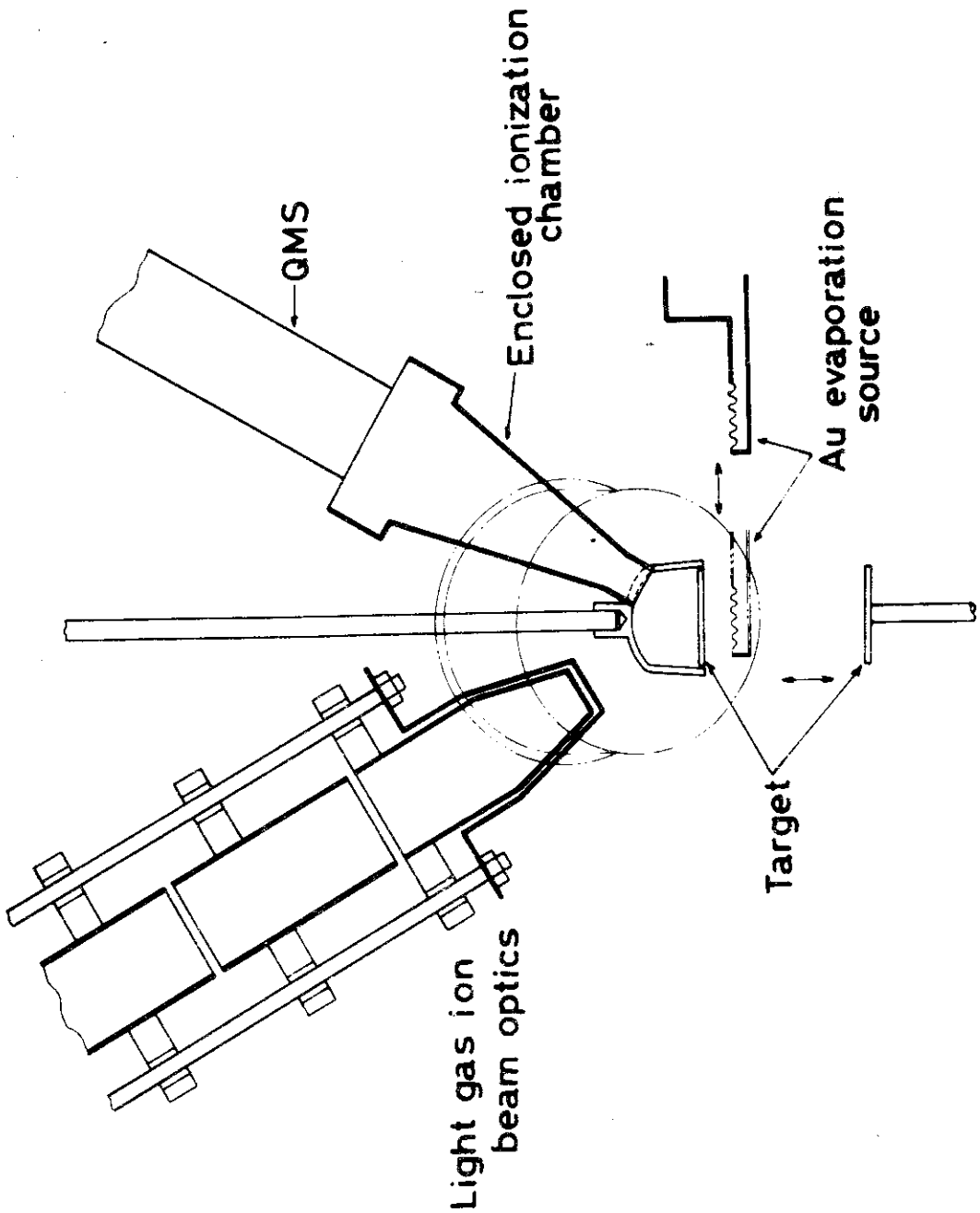

Fig.8 Set-up for measurements of gas release during light gas ion bombardment and thermal desorption of trapped molecules.

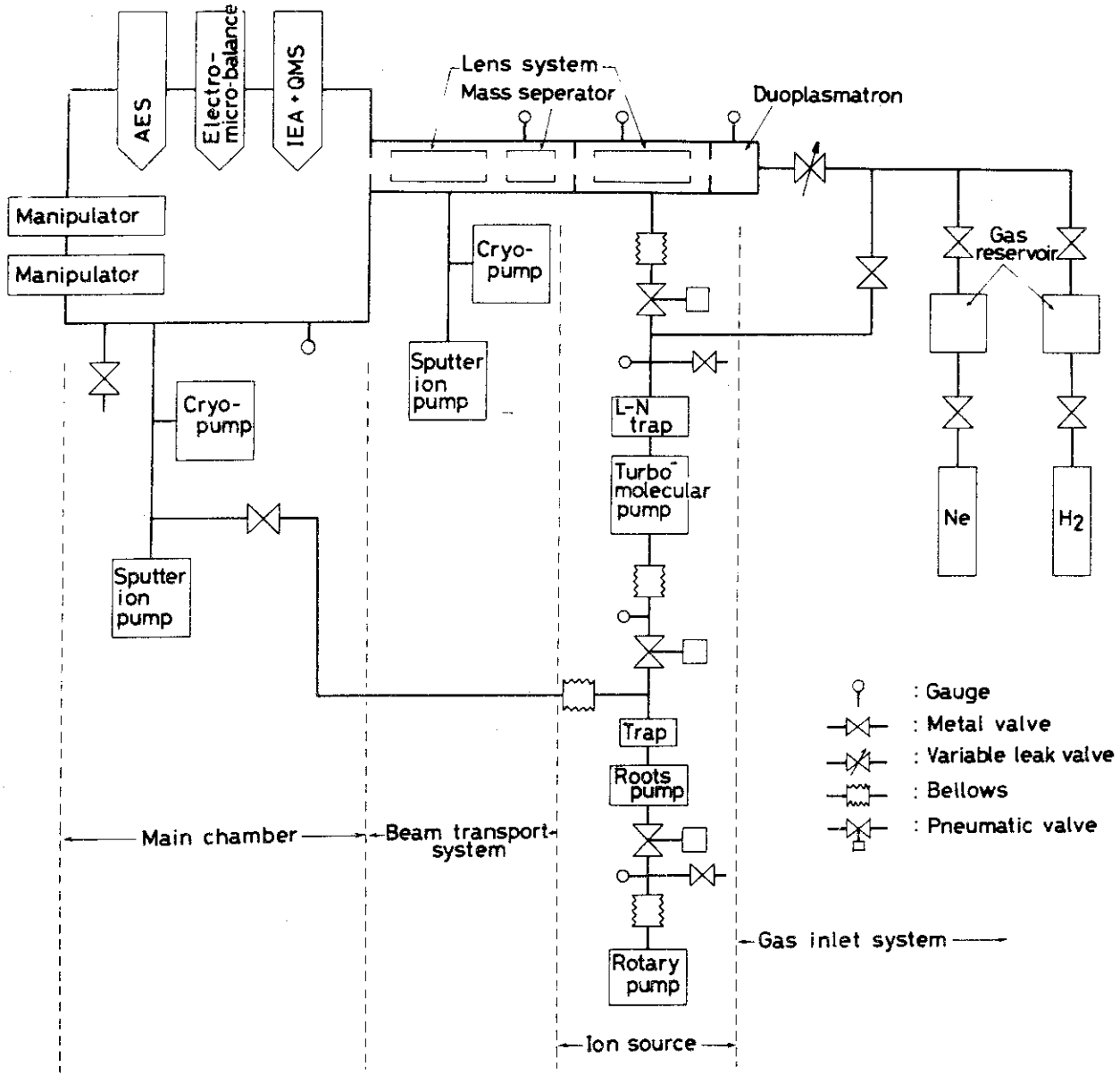

Fig.9 Pumping system.

Electrode	Voltage	Proton beam energy	
		0.1 keV	6 keV
EL 0	VL 0	+0.1	+6
EL 1	VL 1	-2.9	+3
EL 2	VL 2	-6	-6
EL 3	VL 3	-0.4	+5
EL 4	VL 4	〃	〃
EL 5	VL 5	〃	〃
EL 6	VL 6	〃	〃
EL 7	VL 7	-2	-2
EL 8	VL 8	-0.4	+5
EL 9	VL 9	〃	〃
EL10	VL10	〃	〃
EL11	VL11	-3	0
EL12	VL12	-0.4	+5
EL13	VL13	〃	〃
EL14	VL14	〃	〃
EL15	VL15	-3	0
EL16	VL16	-0.4	+5
EL17	VL17	0	0

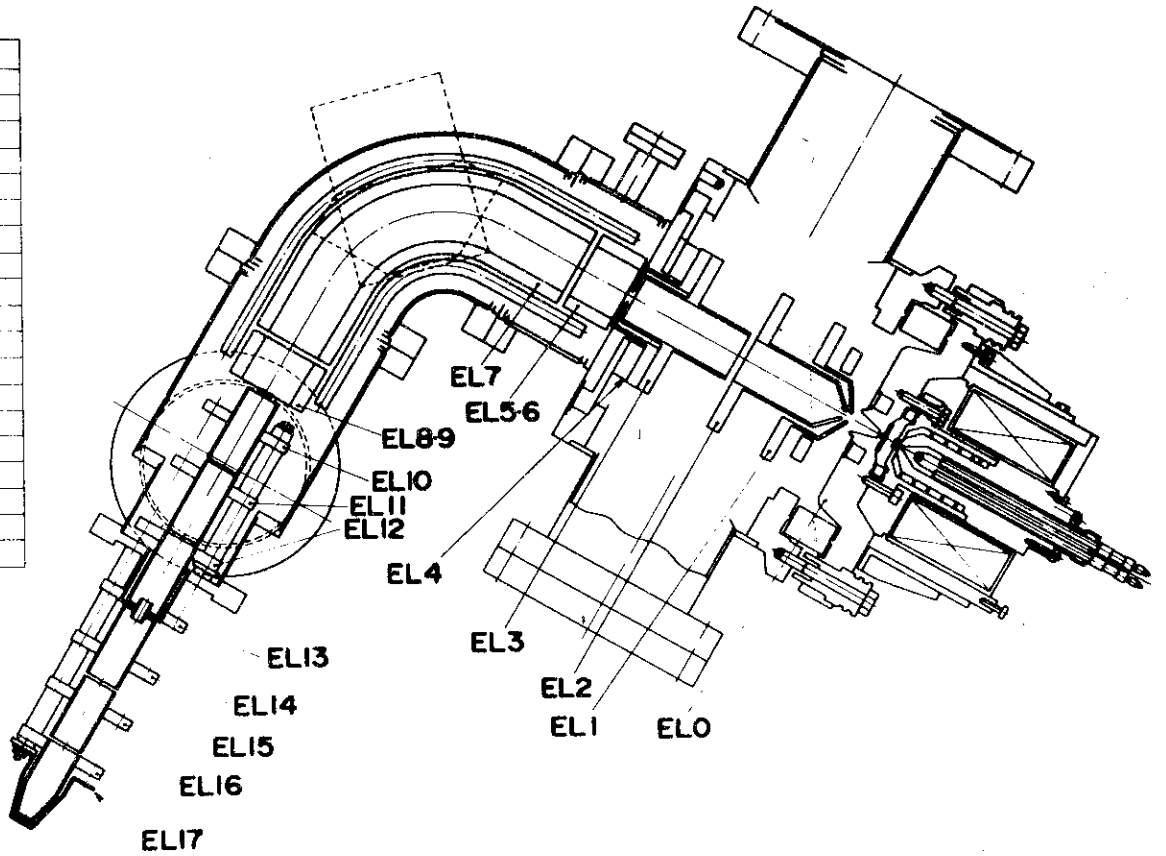

Fig.10 Notation of electrodes and applied voltages.

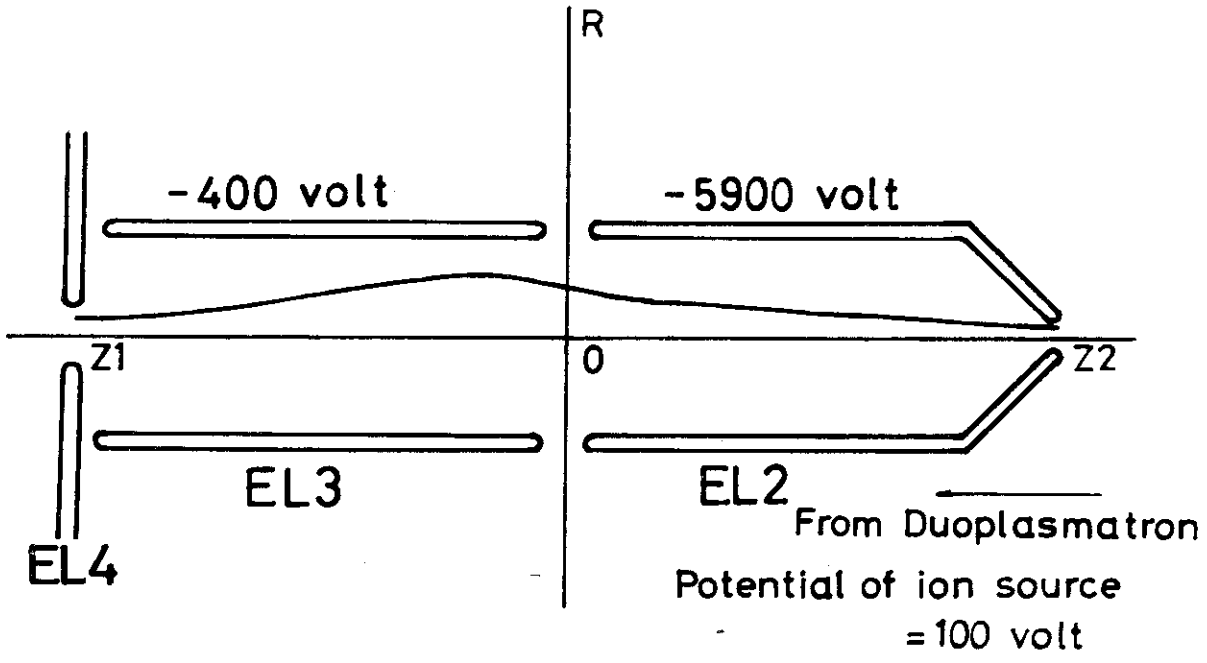

Fig.11 Contour of hydrogen ion beam (H^+; 50%, H_2^+; 50%) in a cylindrical lens.

Mass number: 1.510914.
Radius of lens cylinder: 15.0 mm.
Ion current: 250.0 μA.

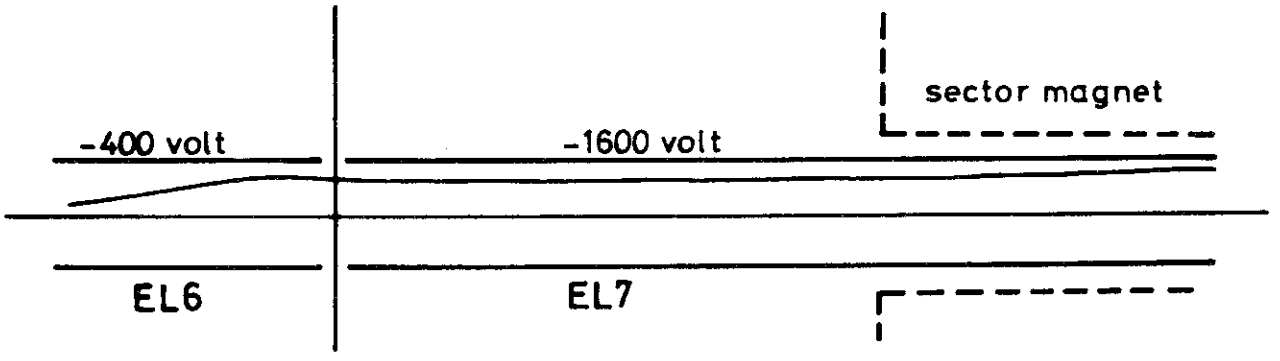

Fig.12 Contour of proton beam in a two-dimensional lens with two electrodes EL6 and EL7.

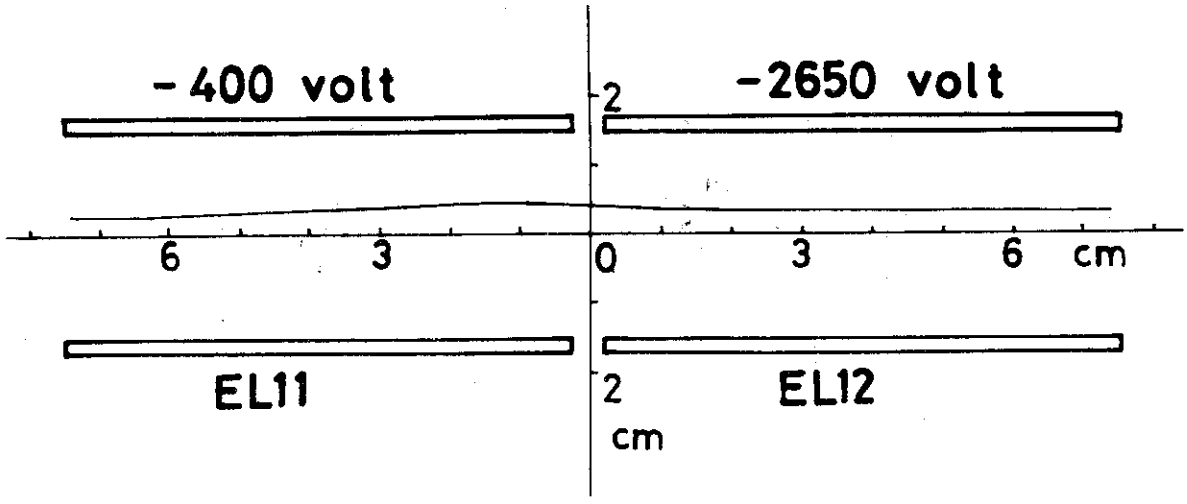

Fig.13 Contour of proton beam in a cylindrical lens with two electrodes EL11 and EL12.

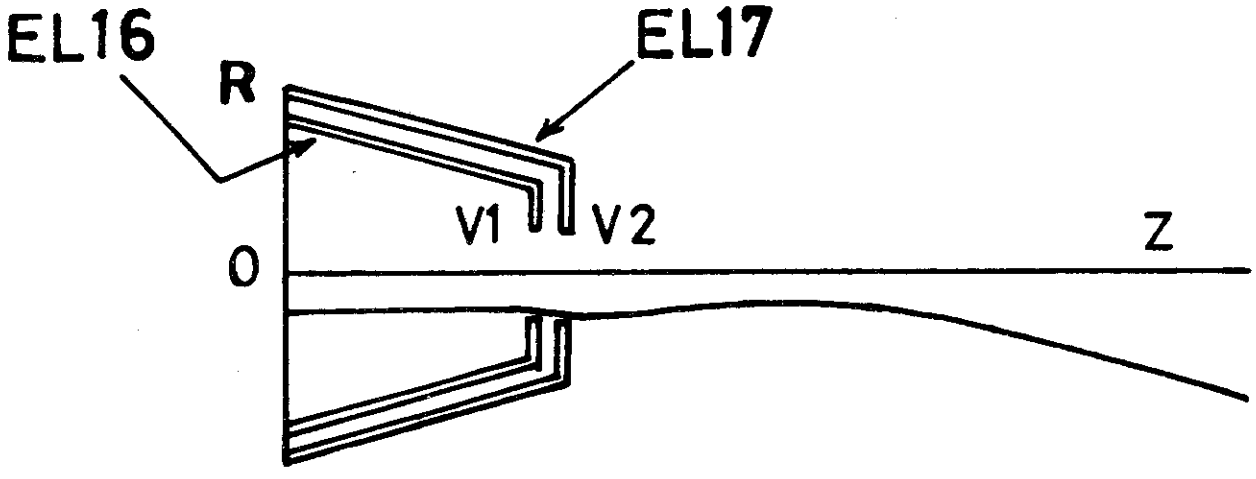

Fig.14 Contour of proton beam passing through a lens with two diaphragms EL16 and EL17.

Diameter of lens slit; 9.0 mm.
Thickness of diaphragms; 1.2 mm.
Separation between diaphragms; 1.8 mm.
Ion current; 60.0 μA.
Beam radius becomes minimum (R_{min} = 3.2905) at Z=50.9697 mm, and spreads by the space charge effect.

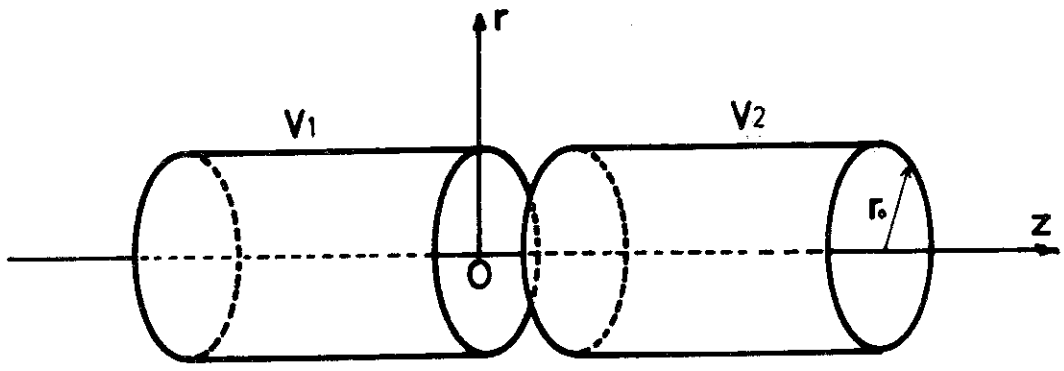

Fig.15 Cylindrical lens.

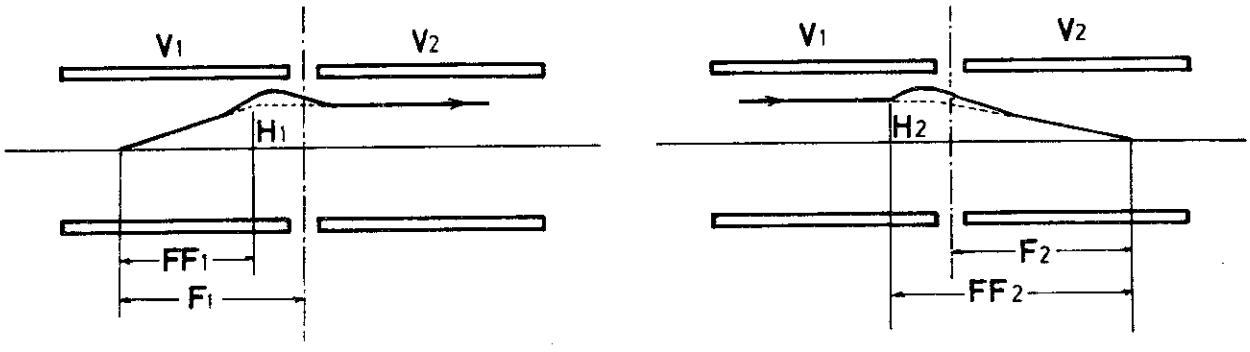

Fig.16 Four kinds of focal length of a cylindrical lnes.

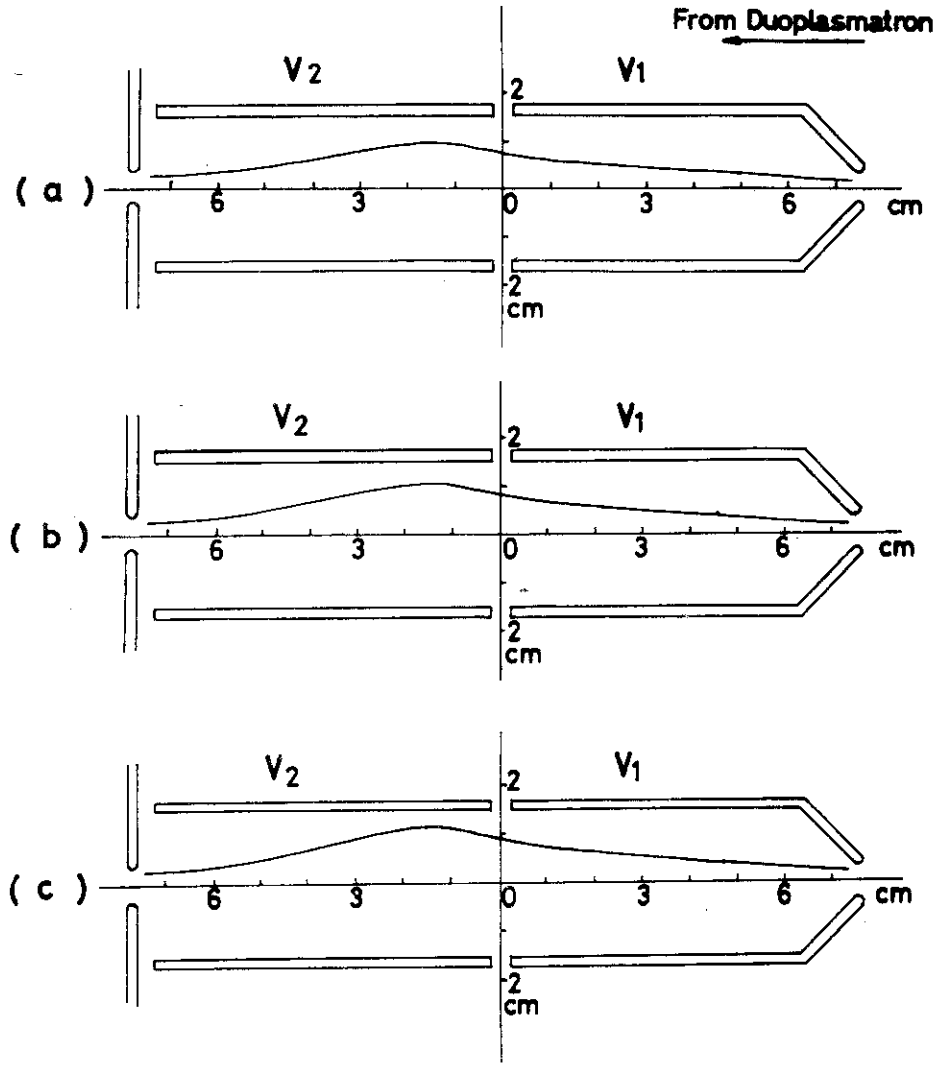

Fig.17 Contour of hydrogen ion beam (H^+; 50%, H_2^+; 50%) in a cylindrical lens.

Mass number; 1.510914
Radius of lens cylinder; 15.0 [mm]
Potential of ion source; 100 [V]
V_1; -5900 [V]
V_2; -400 [V]

a. Ion current; 250 [μA]
b. Ion current; 300 [μA]
c. Ion current; 350 [μA]

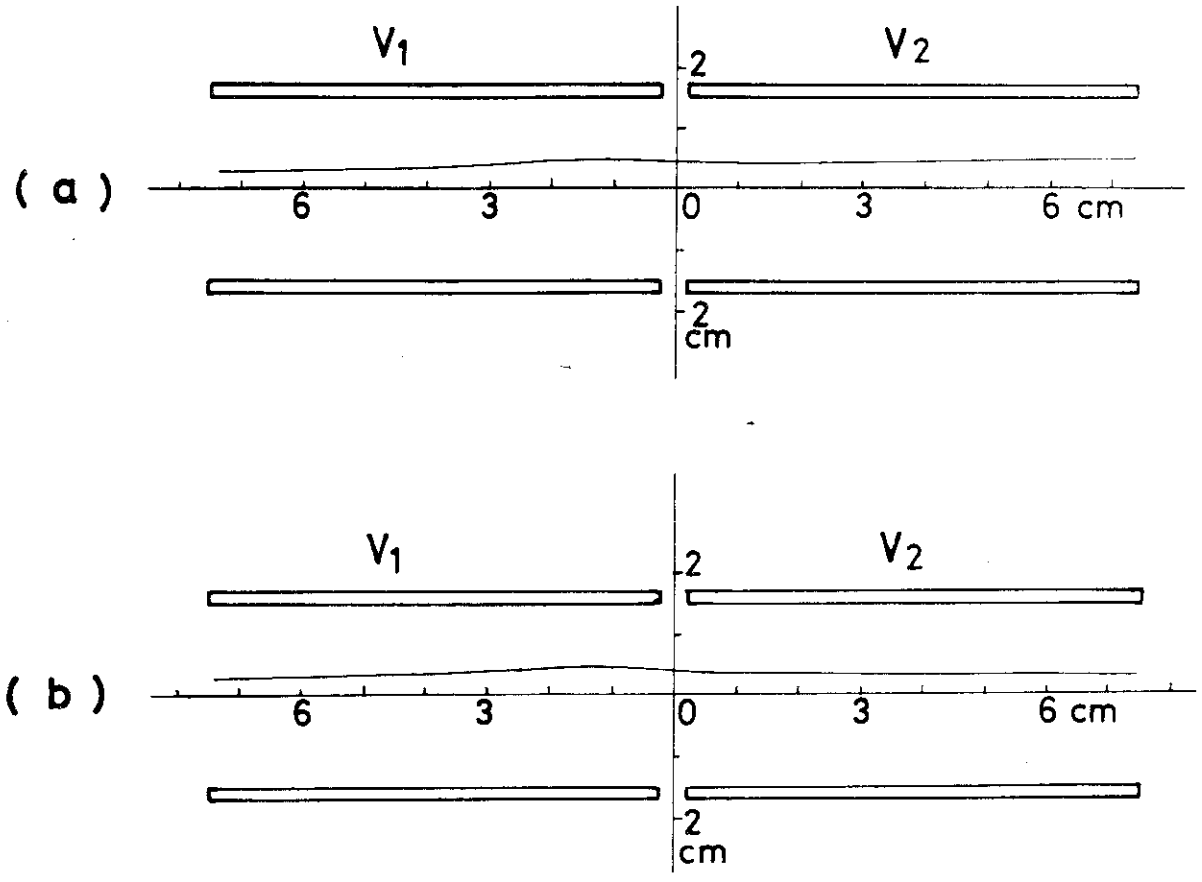

Fig.18 Contour of proton beam in a cylindrical lens.

Radius of lens cylinder; 15.0 [mm].
Ion current: 60 [μA].
Potential of ion source; 100 [V].

a) V_1; -400 [V].
   V_2; -1900 [V].
b) V_1; -400 [V].
   V_2; -2650 [V].

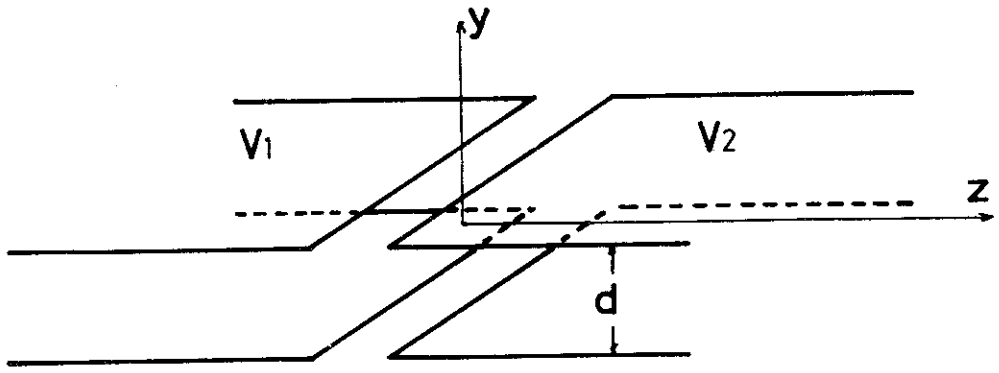

Fig.19 Two-dimensional lens.

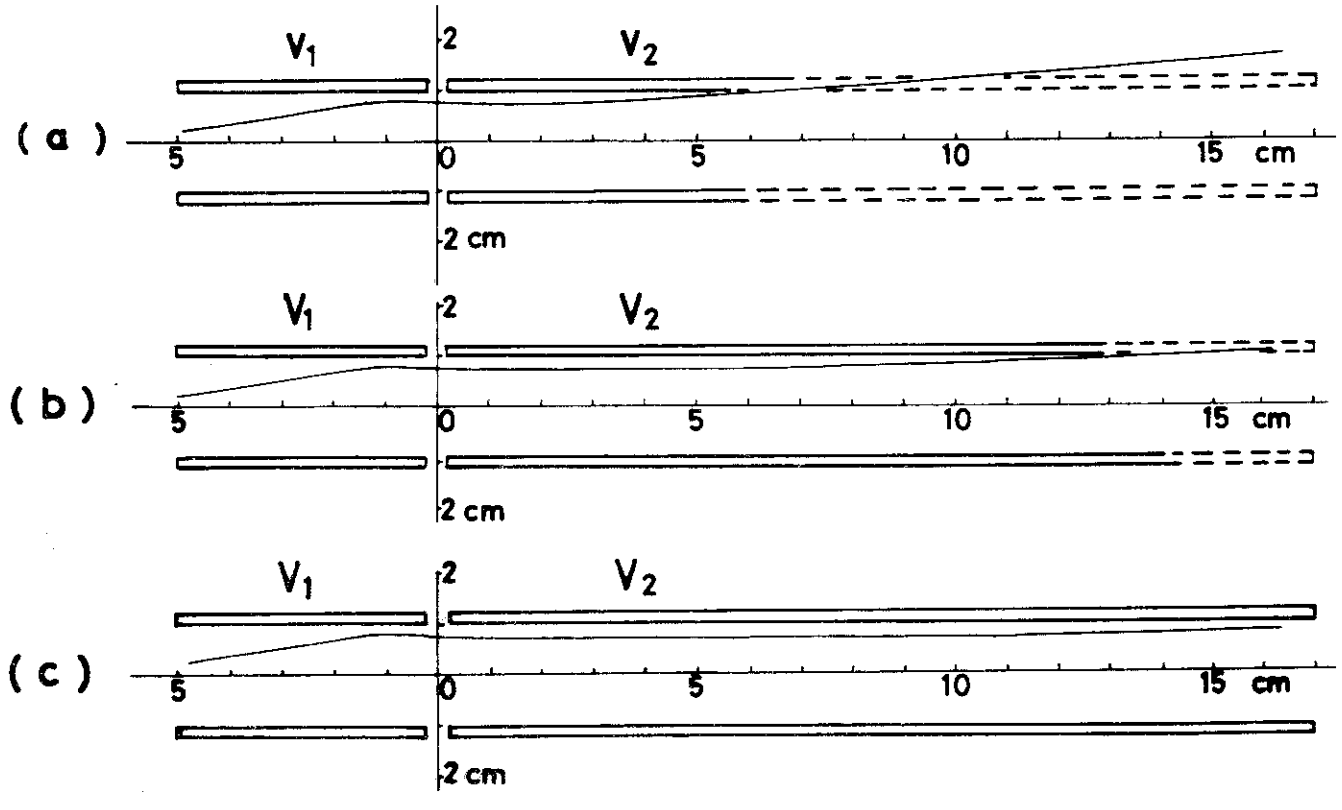

Fig.20 Contour of proton beam in a two-dimensional lens.

Distance between parallel electrodes d; 20 [mm]
Ion current; 60 [μA]
Potential of ion source; 100 [V]

a. V_1; -400 [V], V_2; -1300 [V]
b. V_1; -400 [V], V_2; -1500 [V]
c. V_1; -400 [V], V_2; -1600 [V]

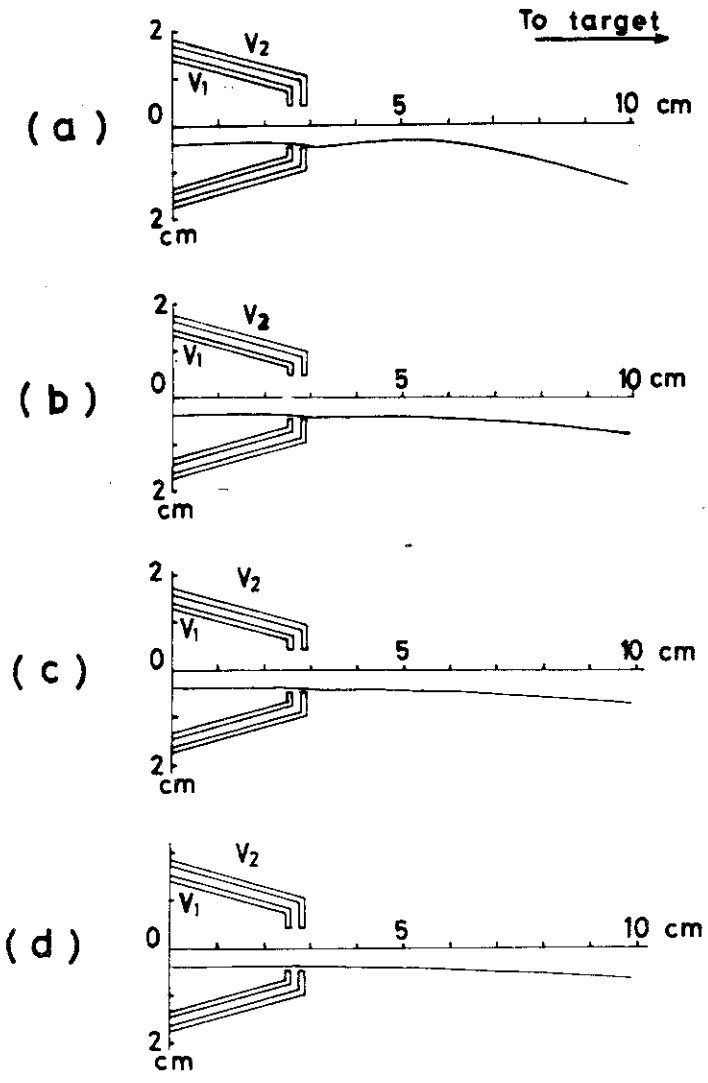

Fig.21 Contour of proton beam passing through a lens with two diaphragms.

Diameter of lens slit; 9.0 [mm]
Thickness of diaphragms; 1.2 [mm]
Separation between diaphragms; 1.8 [mm]
Ion current; 60 [μA]

a. Potential of ion source; 100 [V]
V_1; -400 [V]
V_2; 0 [V]

b. Potential of ion source; 200 [V]
V_1; -300 [V]
V_2; 0 [V]

c. Potential of ion source; 300 [V]
V_1; -200 [V]
V_2; 0 [V]

d. Potential of ion source; 400 [V]
V_1; -100 [V]
V_2; 0 [V]